

Excellent cycling stability with high SnO₂ loading on a three-dimensional graphene network for lithium ion batteries



Miao Zhang^a, Zhenhe Sun^a, Tengfei Zhang^a, Dong Sui^a, Yanfeng Ma^a,
Yongsheng Chen^{a, b, *}

^a Centre for Nanoscale Science and Technology, Collaborative Innovation Center of Chemical Science and Engineering (Tianjin), School of Materials Science and Engineering, Nankai University, Tianjin 300071, China

^b Key Laboratory of Functional Polymer Materials and the Institute of Polymer Chemistry, College of Chemistry, Nankai University, Tianjin 300071, China

ARTICLE INFO

Article history:

Received 6 December 2015

Received in revised form

31 January 2016

Accepted 9 February 2016

Available online 11 February 2016

ABSTRACT

Carbon materials, including pyrolytic carbon and nanocarbon, especially graphene, have been reported to be introduced in the SnO₂-based anodes to decrease the capacity decay during cycling, but the capacity fading was not effectively suppressed. Herein, we report a three-dimensional cross-linked graphene material as the template to load electrochemically active material SnO₂. A 3D composite of graphene and SnO₂ was obtained with a relatively higher SnO₂ loading of 89.51 wt%. The material shows excellent cycling stability with high reversible specific capacity (97% capacity retention, *ca.* 1096 mA h g⁻¹ after 150 cycles at 1 A g⁻¹ with 95% capacity retention, and *ca.* 1073 mA h g⁻¹ after 500 cycles at 1 A g⁻¹). Furthermore, its specific capacity remains at around 610 mA h g⁻¹ at a high current density of 5 A g⁻¹ (fully charged in ~15 min).

© 2016 Elsevier Ltd. All rights reserved.

1. Introduction

Alloying type anode materials such as Si, Ge and Sn, which have superior theoretical lithium storage capacity, are considered as prospective anode materials to provide much higher energy density of next generation lithium ion batteries (LIBs) for applications, such as electronic devices, handy power tools, electric vehicles, and communication equipment [1–5]. Since metal oxides are easier to handle and process in comparison to corresponding elements and metals [6], oxides such as tin dioxide (SnO₂) have attracted considerable attention. The alloying and conversion lithiation mechanism of SnO₂ renders it a high theoretical capacity of 1494 mA h g⁻¹, corresponding to 8.4 mol lithium in total [7]. In addition, SnO₂ possesses merits such as low cost, abundance, environmental benignity and so on. However, SnO₂ anodes undergo large volume changes during the lithium insertion and extraction process (~300%), which is detrimental to the long-term lithium ion cycling since it will give rise to “electrochemical pulverization” of the active material [8], resulting in loss of electrical

contact between the active materials and the current collector. This shortcoming results in the rapid capacity fading. Furthermore, the unstable solid state interface (SEI) films will decrease the capacity even though particle pulverization restrained, which will further impair the cycling stability.

Recently, extensive researches of SnO₂ as the anode materials had been conducted, especially for improving the electrochemical cycling performance. One approach is building pristine SnO₂ with rational design of hierarchical structures [9,10], sheets [11,12], or hollow nanostructures [13–16]. Another way is to introduce SnO₂ into a buffer layer matrix to overcome the volume expansion. Carbonaceous materials including pyrolytic carbon and graphene are the most explored buffer layer. Graphene, due to its large surface area, mechanical flexibility, chemical stability and excellent conductivity, is attracted extensive research interests in improving the cycling performance of SnO₂ anodes [17,18]. These SnO₂/graphene composites mostly denoted as SnO₂/rGO in which rGO represents graphene reduced from graphene oxide, exhibiting better electrochemical performance than pristine SnO₂, but initial decay always exists [19,20]. Scientists are trying hard to increase both the capacity and stability in the whole long cycling process. When adjusting the crystallinity of SnO₂ from crystalline to amorphous, the later one was more effective than the former one in overcoming electrochemical and mechanical degradation for the intrinsically isotropic nature of amorphous SnO₂ [21]. The addition of dopants

* Corresponding author. Key Laboratory of Functional Polymer Materials and the Institute of Polymer Chemistry, College of Chemistry, Nankai University, Tianjin 300071, China.

E-mail address: yschen99@nankai.edu.cn (Y. Chen).

or other coating materials into the SnO₂/graphene composites could also promote the electrochemical performance. For example, N-doping graphene composites, which further suppress the aggregation of Sn nanoparticles during the lithiation process and enhance the conversion reaction of SnO₂ nanocrystals, can improve the reversibility of the lithium electrochemical activity of SnO₂ [22–24]. Good cycling performance with a reversible charge capacity of 1346 mA h g⁻¹ after 500 cycles at 0.5 A g⁻¹ has been achieved, much better than that of SnO₂/rGO with only 500 mA h g⁻¹ after 200 cycles [24]. The LIB anodes prepared by using the F-doping SnO₂ on surface of rGO sheets, which both enhanced electron transportation and lithium ion diffusion, exhibited a specific capacity of 1277 mA h g⁻¹ after 100 cycles [25]. Amorphous carbon [26] and conductive polymers [27,28] were also utilized to further coat on the SnO₂/graphene composite to immobilize the SnO₂, decrease the particles aggregation and suppress the continuous SEI film growth, thus also improved the cycling stability.

These methods above provide basically good cycling stability, but the absolute electrochemical capacity is not sufficiently high and still suffers from decay during the initial ten or twenty cycles. The fabrication of SnO₂/graphene composite electrode material with both high capacity and stable cycling simultaneously is still a great challenge, particularly for the case with high SnO₂ loading [23] (Table S1 in supporting information).

In this work, we designed a SnO₂ nanoparticle and three-dimensional (3D) graphene composite (SnO₂@3DG) with high SnO₂ loadings (up to 89.51 wt%). The SnO₂@3DG composite has a hierarchical structure where the graphene sheets assembled into 3D architecture and the SnO₂ nanoparticles decorated uniformly on the graphene walls. The 3DG provides a robust three-dimensional structure and proper pore size to accommodate the large volume change of SnO₂ nanoparticles, and the continuous graphene network of electrode material also provides better electrical conductivity and more effective lithium ion diffusion path. Therefore, the SnO₂@3DG with near 90% loading of SnO₂ exhibits excellent electrochemical performance, with a high capacity of ca. 1096 mA h g⁻¹ after 150 cycles at 1 A g⁻¹ with 97% capacity retention, and ca. 1073 mA h g⁻¹ after 500 cycles at 1 A g⁻¹ with 95% capacity retention.

2. Experimental section

2.1. Materials synthesis

2.1.1. Synthesis of 3DG

All the materials were used as purchased unless otherwise indicated. Graphene oxide (GO) was synthesized from natural flake graphite (average particle diameter of 300 μm, 99.95% purity, Qingdao Huarun Graphite Co., Ltd.) by a modified Hummers' method [29]. Then the GO dispersion (2 mg mL⁻¹) and ethanol (99.5%) were homogeneously mixed at a volume ratio of 1:1 (100 mL:100 mL) with intense agitation to form the GO alcohol-hydrogel. The GO alcohol-hydrogel was poured into 100 mL Teflon-lined stainless steel autoclave and heated to 180 °C for 12 h. The 3DG was obtained after solvent exchange and freeze-dried, and finally annealing at 400 °C for 2 h with a heating rate of 1 °C min⁻¹ under a H₂/Ar (5:95 v/v) atmosphere.

2.1.2. Synthesis of SnO₂ nanoparticles

SnO₂ nanoparticles were prepared using a similar method to what was previously reported [30]. 700 mg of SnCl₂·2H₂O (Tianjin Guangfu Fine Chemical Research Institute) were added into 100 mL of ethanol/water mixture solvent (1:1 v/v) with intense agitation. Then, 6 M KOH solution was slowly added into the solution until

pH = 7. The milk-like liquid was poured into 100 mL Teflon-lined stainless steel autoclave and heated to 180 °C for 12 h. The resultant was washed and freeze-dried, and finally annealing at 400 °C for 2 h with a heating rate of 1 °C min⁻¹ under a H₂/Ar (5:95 v/v) atmosphere to get the final SnO₂ nanoparticles.

2.1.3. Synthesis of SnO₂@3DG composites

The GO alcohol hydrogel and a certain amount of SnCl₂·2H₂O (Tianjin Guangfu Fine Chemical Research Institute) were homogeneously mixed at a mass ratio of 1:10 with intense agitation. After 5 min, 6 M KOH solution was slowly added into the solution until pH = 7. Then the viscous liquid was poured into 100 mL Teflon-lined stainless steel autoclave and heated to 180 °C for 12 h. The SnO₂@3DG cylindrical resultant was washed and freeze-dried, and finally annealing at 400 °C for 2 h with a heating rate of 1 °C min⁻¹ under a H₂/Ar (5:95 v/v) atmosphere to obtain the SnO₂@3DG composites [30].

2.2. Characterization

Transmission electron microscopy (TEM) was performed using a JEOL TEM-2100 electron microscope operated at 200 kV. The morphology of the 3DG was observed by scanning electron microscopy (Nova NanoSEM 230 operated at 10.0 kV). Powder X-ray diffraction (XRD) analysis was performed on a Rigaku D/Max-2500 diffractometer with Cu Kα radiation. Thermogravimetric (TG) measurements (Netzsch-STA 449C) were conducted from room temperature to 800 °C at a heating rate of 10 °C min⁻¹ in air. X-ray photoelectron spectroscopy (XPS) was carried out using AXIS HIS 165 spectrometer (Kratos Analytical) with a monochromatized Al Kα X-ray source (1486.71 eV photons) to analyze the chemical composition of the products. The nitrogen adsorption/desorption analysis was done at 77 K on a Micromeritics ASAP 2020 apparatus.

2.3. Cell fabrication and electrochemical characterization

Electrochemical measurements were carried out using coin-type cells. To prepare working electrodes, SnO₂@3DG composite, Super P carbon black, and poly(vinylidene fluoride) (PVDF, in N-methyl-2-pyrrolidone) with mass ratio of 80:10:10 were mixed to produce a homogeneous slurry and coated onto a 10 μm thick Cu foil. After heating at 60 °C for 3 h and 150 °C for 1 h under vacuum, the electrode sheet was pressed and punched into ~11 mm diameter electrodes with a mass loading of ~1.25 mg. The coin-type cells were assembled in an argon-filled glove box with lithium metal foil as the counter/reference electrode. And the electrolyte was used as purchased from CAPCHEM Co., Ltd, Shenzhen, China (Part No. LBC3401A4, 1 M LiPF₆ in EC/DEC (1:1 v/v) as the electrolyte with 10% of fluoroethylene carbonate (FEC) as electrolyte additive). The charge/discharge measurements were performed using a battery test system (LAND CT2001A model, Wuhan LAND Electronics. Ltd.) over a voltage window from 0.01 to 3.00 V at room temperature. For the high current density cycle performance, the electrode was pretreated after conditional cycling. For example, the electrode, which was intended to cycle under 1 A g⁻¹, would be previously cycled after two charge–discharge cycles at the current density of 0.1 A g⁻¹ and two charge–discharge cycles at the current density of 0.5 A g⁻¹. Similarly, the electrode supposed to cycle at 0.5 A g⁻¹, would be previously cycled after two charge–discharge cycles at the current density of 0.1 A g⁻¹. Cyclic voltammetry (CV) and Electrochemical impedance spectral (EIS) measurements were recorded using an Autolab system (Metrohm). CV tests were carried out in a scan rate of 0.1 mV s⁻¹ at potential ranges of 0.01–3.00 V. EIS measurements were carried out at AC amplitude of 10 mV in the range of 100 kHz–10 mHz.

3. Results and discussion

3.1. Morphological and structural studies

The composites with different loadings (~46–91%) of SnO₂ were synthesized from different ratios of graphene and SnO₂, and the rate performance results are shown in Fig. S1. The optimized and relatively high loading of SnO₂ of 89.51 wt% (determined by the thermogravimetric analysis, Fig. 1a) demonstrated the highest capacity and was selected and studied further. Fig. 1b shows the XRD patterns of the as-prepared 3DG, SnO₂@3DG, together with that of the pristine SnO₂ nanoparticles. The peaks of the SnO₂@3DG composites are identical with those of the SnO₂ nanoparticles, confirming the presence of tetragonal rutile-like SnO₂ (JCPDS Card No. 41–1445). Furthermore, 3DG exhibits a very weak and extremely broad (002) peak in the range of 24–28°, indicating almost no or very weak long-range graphene sheet re-stacking [31]. The X-ray photoelectron spectroscopy (XPS) of SnO₂@3DG is shown in Fig. 2, where two peaks at 487.2 and 495.6 eV were observed and are attributable to Sn 3d_{5/2} and Sn 3d_{3/2} spin-orbit peaks of SnO₂, confirming the formation of SnO₂ nanoparticles on the surface of graphene sheets. Fig. 2c displays the spectra of C 1s of SnO₂@3DG composite. The C 1s region of graphite oxide gives two components at around 284.6 and 286.8 eV, which can be generally assigned to the C–C and C–O components, indicating that most of the oxygenated functional groups on graphene oxide have been removed during hydrothermal process. In addition, based on experimental nitrogen adsorption data, the pore-size distribution (Fig. 3b) of this material is analyzed using a non-local density functional theory (NL-DFT) method, showing that the pore distribution of the hybrid material from 2 to 75 nm in diameter, which is quite different from previous reports with a narrow pore distribution with small pores (usually less than 5 nm) [32]. Nano-composite electrode materials with wide pore size distribution can effectively accommodate volume change and is beneficial for electrolyte access, thus contributes to the high capacity and excellent cycling performance. The specific surface area (SSA) was calculated by the BET method based on adsorption data in the relative pressure (P/P₀) (Fig. 3a). Despite a large percentage of SnO₂ was introduced on graphene walls, the specific surface area (SSA) of the product is as high as 126 m² g⁻¹.

After the solvothermal reaction and high-temperature annealing, both 3DG and SnO₂@3DG are formed as cylindrical bulk 3DG (shown in the insets of Fig. S2a and Fig. 4b, respectively). A schematic of the structure of the SnO₂@3DG composite is shown in Fig. 4a. The SEM images of SnO₂@3DG (Fig. 4b) shows it is highly

porous material. Fig. 4c is the enlarged image of (Fig. 4b) and shows that the cross-linked part of the graphene walls, in which the graphene sheets randomly arranged and pores are constructed. As shown in Fig. 4c, graphene sheets vertically or aslant linked with each other rather than stacked with each other. This structure shows SnO₂@3DG should be a three-dimensional crosslinked monolithic graphene material, where the graphene sheets, as the building unit, are covalently crosslinked together through reactions between the oxygenic functional groups located mostly on the sheets edges during the solvothermal process and the bivalent tin ions reduce the GO sheets and adhere on it the same time [33–35]. Thus, this SnO₂@3DG structure should be quite different from the previous reports of SnO₂@Graphene composites [12,36–39], where the no three-dimensional crosslinked monolithic structure exist. This would be more beneficial for volume change and lithium ion transportation, thus good cycling stability at high rate. From the TEM image presented in Fig. 4d, it is obvious that large quantities of SnO₂ nanoparticles are uniformly dispersed on the graphene sheets. The nanoparticles on the graphene sheets with diameter of ~20 nm in Fig. 4c echoes the nanoparticle cluster (the structures labeled with yellow lines) in Fig. 4d. In the selected-area electron diffraction (SAED) pattern (inset of Fig. 4d), four distinct diffraction rings represent (110), (101), (200), and (211), confirming the tetragonal rutile-like crystal form of SnO₂ (JCPDS Card No. 41–1445), which is consistent with the XRD pattern (Fig. 1b). High resolution transmission electron microscope (HRTEM) investigation (Fig. 4e) displays SnO₂ nanocrystals bound in graphene sheets with sizes of ~5 nm. The distance of 0.33 nm can be identified as (110) of SnO₂ nanoparticles. The structural uniformity of SnO₂ nanocomposites on 3DG may offer an excellent mechanical integrity. Thus, such an unparalleled structure of SnO₂@3DG would be expected to have superior performance for lithium storage.

3.2. Electrochemical performances

The cyclic voltammetry (CV) curves of the first three cycles of the SnO₂@3DG electrode under a scan rate of 0.1 mV s⁻¹ at potential ranges of 0.01–3.00 V vs Li⁺/Li are shown in Fig. 5a. In the first negative scan (lithium ion insertion process), the cathodic peaks at 0.83 V disappeared in the following anodic scan, corresponding to the formation of the solid electrolyte interphase (SEI). From the second and third scan, the CV behavior is generally consistent with that reported previously [8,40]. Specifically, three characteristic pairs of redox peaks are clearly observed at the potential of (0.09 V, 0.58 V), (0.39 V, 1.30 V), and (1.17 V, 2.01 V). The first pair is ascribed to the reversible alloying and dealloying

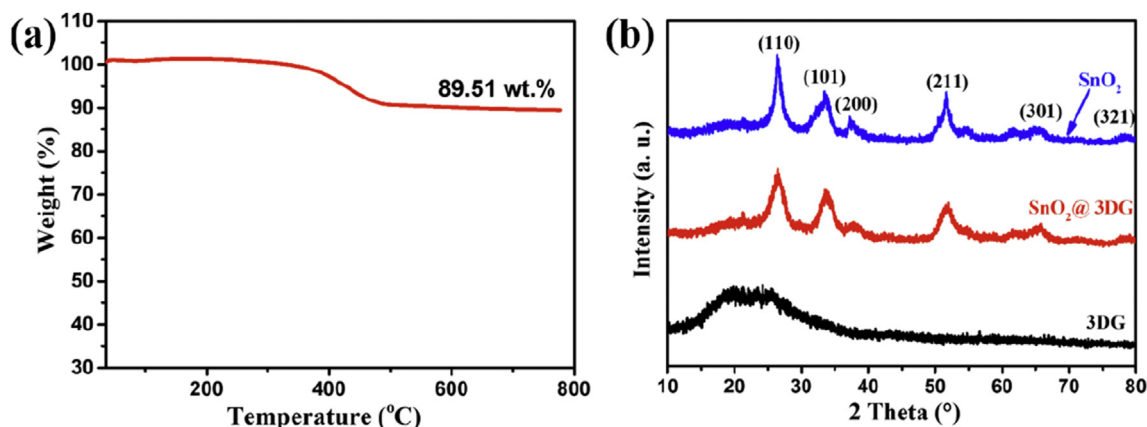


Fig. 1. (a) Thermogravimetric curves of SnO₂@3DG material in air with a heating rate of 10 °C min⁻¹; (b) XRD profiles of SnO₂ nanoparticle, 3DG and SnO₂@3DG. (A colour version of this figure can be viewed online.)

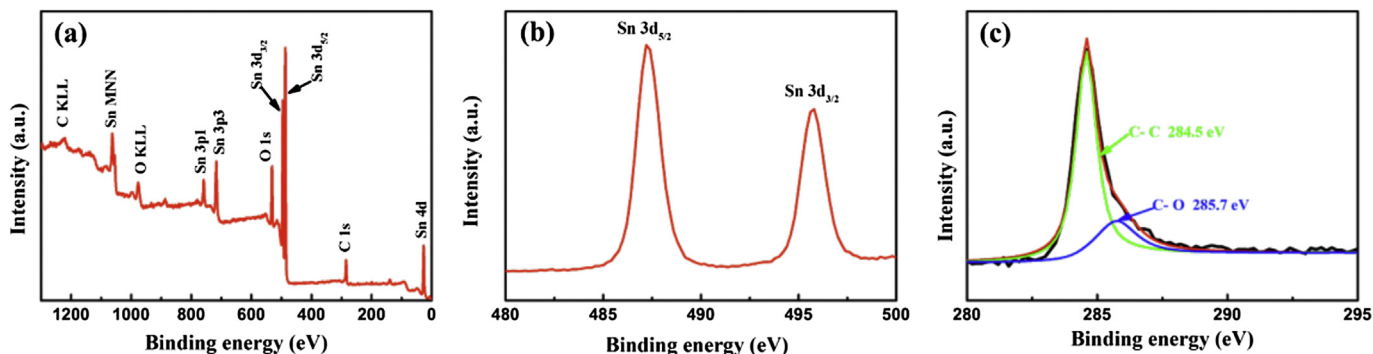


Fig. 2. (a) XPS survey scan of SnO₂@3DG; (b) The XPS spectra of the Sn 3d peaks of the SnO₂@3DG; (c) The XPS spectra of the C1s peaks of the SnO₂@3DG. (A colour version of this figure can be viewed online.)

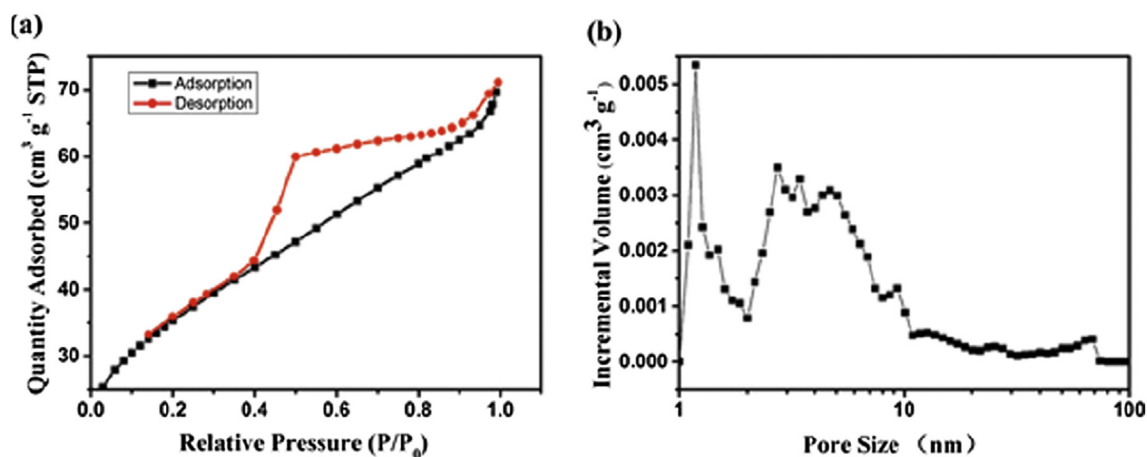
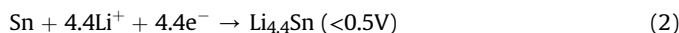


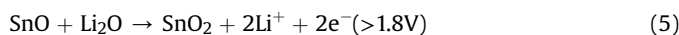
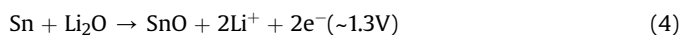
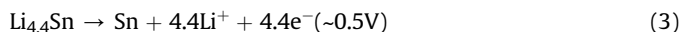
Fig. 3. (a) Nitrogen adsorption/desorption isotherms of SnO₂@3DG; (b) Pore-size distribution plot calculated using the DFT method. (A colour version of this figure can be viewed online.)

reaction according to Eq. (2) and (3), shown below, while the two peaks at 1.30 V and 2.01 V are related to the conversion reaction depicted in Eq. (4) and (5). The above two peaks are more obvious than previous reports [19,20,24], which enable our composite to exhibit higher capacity. This fully conversion reaction of SnO₂ and the good cycling stability are resulted from the unique and characteristic structure of 3D graphene framework with chemically bonded and cross linked graphene sheets, which enable retaining the overall morphology stability of the electrode and thus cycling stability.

Li⁺ insertion process



Li⁺ extraction process



The lithium lithiation/delithiation profiles of the SnO₂@3DG electrode at a current density of 0.1 A g⁻¹ in a voltage range of 0.01–3.00 V are shown in Fig. S3. Three slope regions can be

identified in the discharge (lithium insertion) process of the first cycle, and it gives a very high discharge capacity of 1648 mA h g⁻¹ and charge capacity of 1409 mA h g⁻¹ with an initial Coulombic efficiency of 85.51%. This discharge capacity is near the theoretic capacity of the SnO₂@3DG composite (theoretic capacity of this hybrid is calculated as $C_{\text{theoretical}} = C_{\text{SnO}_2} \cdot \% \text{mass of SnO}_2 + C_{\text{Graphene}} \cdot \% \text{mass of Graphene} = 1494 \cdot 0.8951 + 744 \cdot 0.1049 = 1415 \text{ mA h g}^{-1}$), showing a superior lithium storage capacity. The 14.5% capacity loss of the SnO₂@3DG electrode may be mainly ascribed to the formation of the SEI film, similar as reported before [19,20]. Note the specific capacity values are calculated on the basis of the total mass of the SnO₂@3DG hybrid material. Though there is a slight capacity loss in the first cycle, the capacity retention keeps steady during the following cycles. In the second and third charge/discharge cycles, the Coulombic efficiency increases to above 97%.

The rate and cycling performance of 3DG, SnO₂ and SnO₂@3DG are exhibited in the Fig. 5b and c. It can be clearly seen that SnO₂@3DG exhibit good rate capability and maintain a high specific capacity in the current density range of 0.1–5 A g⁻¹ (the specific capacities of SnO₂@3DG remain at around 610 mA h g⁻¹ at 5 A g⁻¹, fully charged in ~15 min), while the SnO₂ nanoparticles show dramatic decay and the 3DG has a low specific capacity despite having excellent rate capability. The same capacity tendency of those three composites also appears in the cycling performance. After conditional cycling, the 3DG electrode delivers a low lithium storage capacity of 189 mA h g⁻¹ after 150 cycles, whereas the

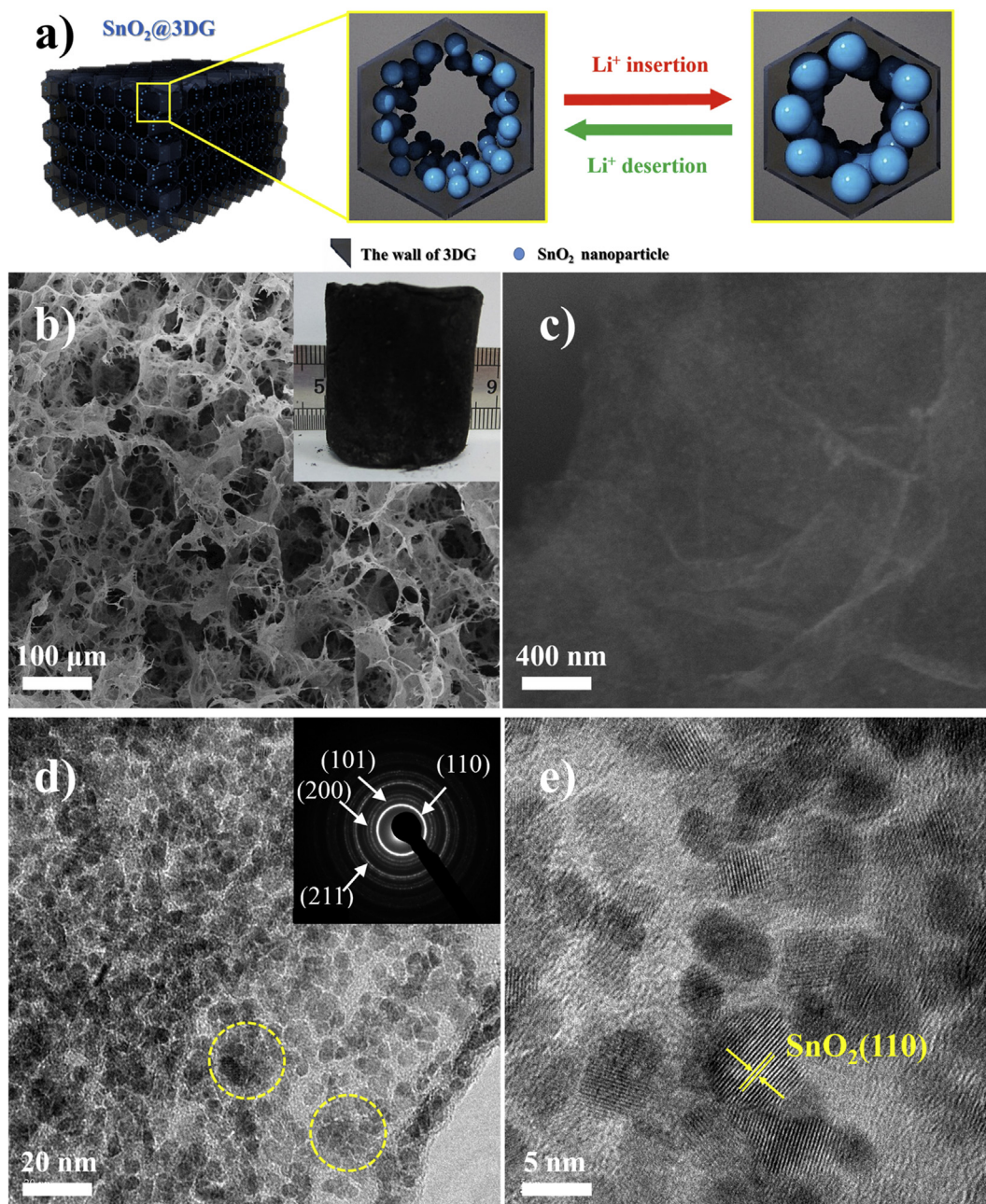


Fig. 4. (a) Schematic of the structure of the SnO₂@3DG composite. (b, c) SEM image of SnO₂@3DG composite (inset of b: the optical image of SnO₂@3DG composite); (d, e) TEM images of SnO₂@3DG composite (inset of d: the corresponding SAED pattern). (A colour version of this figure can be viewed online.)

capacity of pure SnO₂ electrode decays quickly (321 mA h g⁻¹ after 150 cycles) due to its huge volume change. In contrast, the SnO₂@3DG has specific capacity of 1127 mA h g⁻¹ in the initial cycle of 1 A g⁻¹ and it maintains at 1096 mA h g⁻¹ after 150 cycles. The voltage profiles generated by the SnO₂@3DG composite anode in the 1st, 10th, 50th, 100th and 150th cycles at a current density of 1 A g⁻¹ within a voltage window of 0.01–3.00 V are shown in Fig. 5d. Those profiles are nearly overlapped with each other, indicating the excellent cycle performance. These results demonstrates that the stable electrical contact of SnO₂ is retained during cycling despite the drastic volume change, leading to good cycling stability of the composite. Both impedance curves of fresh electrode and after 150 cycles show a compressed semicircle in the high-frequency region and an inclined line in the low-frequency region, which can be assigned to the charge-transfer resistance and

semi-diffusion of lithium ions respectively. The diameter of the semicircle for the fresh SnO₂@3DG electrode is slightly larger than that after 150 cycles (Fig. S4), which means that the SnO₂@3DG electrode has a decreasing resistance for the interfacial electrochemical reaction after charge/discharge cycles.

3.3. Cycling stability testing

The cycling stability of the SnO₂@3DG anode was further tested at 1 A g⁻¹ for 500 cycles as illustrated in Fig. S5a, which indicates both excellent cycle life and high discharge (lithiation) and charge (delithiation) capacities with high Coulombic efficiency. After initial conditioning cycles, the specific capacity stabilizes at ca. 1120 mA h g⁻¹ during 150 cycles and the Coulombic efficiency increases to more than 99% after initial conditioning cycles. Besides, a

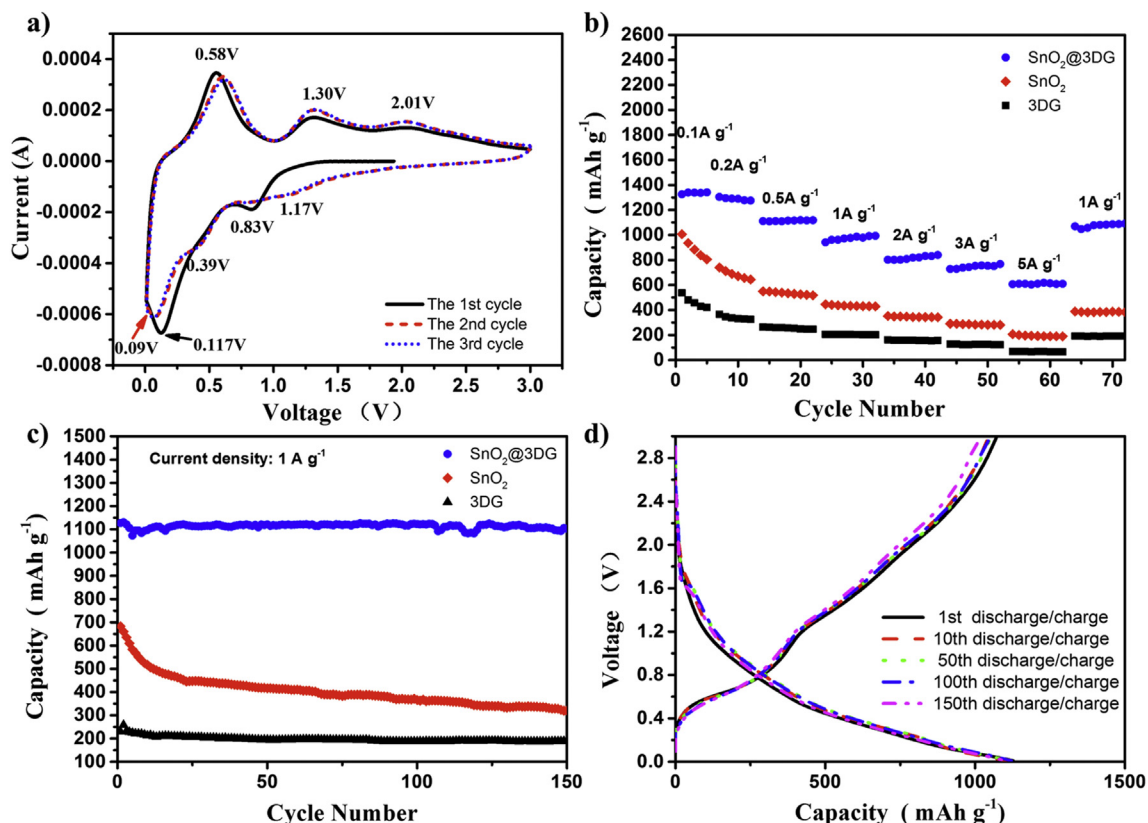


Fig. 5. Electrochemical performance of the SnO₂@3DG composite: (a) CV curves of the first three cycles of the SnO₂@3DG electrode; (b) discharge (lithiation) capacities of the SnO₂ nanoparticles, 3DG and SnO₂@3DG at various rates based on the total weight of active electrode material; (c) cycling performance of the SnO₂ nanoparticles, 3DG and SnO₂@3DG at 1 A g⁻¹ for 150 cycles; (d) The 1st, 10th, 50th, 100th and 150th discharge/charge profiles of the SnO₂@3DG at the current density of 1 A g⁻¹. (A colour version of this figure can be viewed online.)

capacity of 1073 mA h g⁻¹ is obtained after 500 cycles, indicating a high capacity retention of 95%. The capacity still increased slowly to 1401 mA h g⁻¹ after 900 cycles (Fig. S6 and Fig. S7). Note there is a slight increase of the capacity from 300th cycle. While the reason is not clear to us, the ascending capacity may be ascribed to a reversible formation/decomposition of an organic polymeric film from the electrolyte, or an increasing reversibility of the electrochemical reaction between Li₂O and Sn [22,41,42].

Our cycling result was compared with two pioneer earlier works which gave good electrochemical performance at 1 A g⁻¹ as shown in Fig. S5b. In the initial several cycles, the capacities of those two works decreased quickly (~300 mA h g⁻¹ capacity decay from the first cycle to the 20th cycle) and they attain stable cycling performance at a relative low capacity (<1000 mA h g⁻¹) [19,20], whereas our capacity stabilize at ~1100 mA h g⁻¹ even for 100 cycles without obvious capacity decay. As is known to all, most electrode materials demonstrate higher capacity only at a lower current density, such as at 0.5 A g⁻¹. But for comparison, the performance of SnO₂@3DG is also tested at 0.5 A g⁻¹ (Fig. S5c). As is shown in Fig. S5d, the capacity of SnO₂@3DG in the first cycle is close to reported studies, but the cycle performance of SnO₂@3DG has nearly 100% capacity retention even at 100th cycle, compared with only ~67% capacity retention of reported results [16,19,20,24,43] (Fig. S5d).

In order to explore the reasons of the excellent cycling stability and high capacity of the SnO₂@3DG composite, the morphologies of the electrode materials after cycling performance testing were studied. Fig. S8 shows the TEM images of SnO₂@3DG composite after 20 and 150 cycles of discharge/charge tested at 1 A g⁻¹. As can be seen from Fig. S8b and S8d, SnO₂ nanoparticles were uniformly anchored on the graphene sheets and the particle size of the SnO₂

on graphene sheets are unchanged, indicating that the particles were not aggregated and neither pulverized into smaller particles. This might be due to the three-dimensional network of cross-linked graphene sheets, which provides not only the necessary conductivity channel but also the much needed cushion space to accommodate the expanded SnO₂ particles during the changing process [33].

4. Conclusions

In summary, a composite anode material (SnO₂@3DG) was prepared with SnO₂ nanoparticles and three-dimensional (3D) graphene combination with a high SnO₂ loading percent. The material exhibits long-term stability upon cycling with high specific capacity (97% capacity retention, ca. 1096 mA h g⁻¹ after 150 cycles at 1 A g⁻¹ and 95% capacity retention, ca. 1073 mA h g⁻¹ after 500 cycles at 1 A g⁻¹) and superior rate capability (610 mA h g⁻¹ at a high current density of 5 A g⁻¹). This excellent electrochemical performance is believed due to the three-dimensional linked graphene sheet template structure, which enable facilitated ion transportation while keeping the overall electrode morphology stable without significant volume change.

Acknowledgments

The authors gratefully acknowledge financial support from the MOST (Grants 2012CB933401 and 2014CB643502); NSFC (Grants 51273093, 21374050, 51373078, 51422304 and 51472124); NSF of Tianjin City (Grant 13RCGFGX01121).

Appendix A. Supplementary data

Supplementary data related to this article can be found at <http://dx.doi.org/10.1016/j.carbon.2016.02.032>.

References

- [1] J.M. Tarascon, M. Armand, Issues and challenges facing rechargeable lithium batteries, *Nature* 414 (6861) (2001) 359–367.
- [2] M. Armand, J.M. Tarascon, Building better batteries, *Nature* 451 (7179) (2008) 652–657.
- [3] J.B. Goodenough, Energy storage materials: a perspective, *Energy Storage Mater.* 1 (2015) 158–161.
- [4] Z. Li, W. Lv, C. Zhang, J. Qin, W. Wei, J.-J. Shao, et al., Nanospace-confined formation of flattened Sn sheets in pre-seeded graphenes for lithium ion batteries, *Nanoscale* 6 (16) (2014) 9554–9558.
- [5] W. Lv, Z. Li, Y. Deng, Q.-H. Yang, F. Kang, Graphene-based materials for electrochemical energy storage devices: opportunities and challenges, *Energy Storage Mater.* 2 (2016) 107–138.
- [6] P. Poizot, S. Laruelle, S. Grugeon, L. Dupont, J.M. Tarascon, Nano-sized transition-metal oxides as negative-electrode materials for lithium-ion batteries, *Nature* 407 (6803) (2000) 496–499.
- [7] Z.X. Chen, M. Zhou, Y.L. Cao, X.P. Ai, H.X. Yang, J. Liu, In Situ Generation of few-layer graphene coatings on SnO₂-SiC core-shell nanoparticles for high-performance lithium-ion storage, *Adv. Energy Mater.* 2 (1) (2012) 95–102.
- [8] M.V. Reddy, G.V. Subba Rao, B.V. Chowdari, Metal oxides and oxysalts as anode materials for Li ion batteries, *Chem. Rev.* 113 (7) (2013) 5364–5457.
- [9] L. Zhang, G. Zhang, H.B. Wu, L. Yu, X.W. Lou, Hierarchical tubular structures constructed by carbon-coated SnO₂ nanoplates for highly reversible lithium storage, *Adv. Mater.* 25 (18) (2013) 2589–2593.
- [10] H. Wang, A.L. Rogach, Hierarchical SnO₂ nanostructures: recent advances in design, synthesis, and applications, *Chem. Mater.* 26 (1) (2014) 123–133.
- [11] C. Wang, Y. Zhou, M. Ge, X. Xu, Z. Zhang, J.Z. Jiang, Large-scale synthesis of SnO₂ nanosheets with high lithium storage capacity, *J. Am. Chem. Soc.* 132 (1) (2010) 46–47.
- [12] Y. Zhu, H. Guo, H. Zhai, C. Cao, Microwave-assisted and gram-scale synthesis of ultrathin SnO₂ nanosheets with enhanced lithium storage properties, *ACS Appl. Mater. Interfaces* 7 (4) (2015) 2745–2753.
- [13] S. Ding, J.S. Chen, G. Qi, X. Duan, Z. Wang, E.P. Giannelis, et al., Formation of SnO₂ hollow nanospheres inside mesoporous silica nanoreactors, *J. Am. Chem. Soc.* 133 (1) (2011) 21–23.
- [14] Z. Wang, D. Luan, F.Y. Boey, X.W. Lou, Fast formation of SnO₂ nanoboxes with enhanced lithium storage capability, *J. Am. Chem. Soc.* 133 (13) (2011) 4738–4741.
- [15] Y. Yin, S. Xin, L. Wan, C. Li, Y. Guo, SnO₂ hollow spheres: Polymer bead-templated hydrothermal synthesis and their electrochemical properties for lithium storage, *Sci. China. Chem.* 55 (7) (2012) 1314–1318.
- [16] J. Liang, X.Y. Yu, H. Zhou, H.B. Wu, S. Ding, X.W. Lou, Bowl-like SnO₂@carbon hollow particles as an advanced anode material for lithium-ion batteries, *Angew. Chem. Int. Ed.* 53 (47) (2014) 12803–12807.
- [17] X. Huang, X. Qi, F. Boey, H. Zhang, Graphene-based composites, *Chem. Soc. Rev.* 41 (2) (2012) 666–686.
- [18] S.-M. Paek, E. Yoo, I. Honma, Enhanced Cyclic Performance and Lithium Storage Capacity of SnO₂/graphene nanoporous electrodes with three-dimensionally delaminated flexible structure, *Nano Lett.* 9 (1) (2009) 72–75.
- [19] L. Liu, M. An, P. Yang, J. Zhang, Superior cycle performance and high reversible capacity of SnO₂/graphene composite as an anode material for lithium-ion batteries, *Sci. Rep.* 5 (2015) 9055.
- [20] B. Chen, H. Qian, J. Xu, L. Qin, Q.-H. Wu, M. Zheng, et al., Study on SnO₂/graphene composites with superior electrochemical performance for lithium-ion batteries, *J. Mater. Chem. A* 2 (24) (2014) 9345.
- [21] X. Li, X. Meng, J. Liu, D. Geng, Y. Zhang, M.N. Banis, et al., Tin oxide with controlled morphology and crystallinity by atomic layer deposition onto graphene nanosheets for enhanced lithium storage, *Adv. Funct. Mater.* 22 (8) (2012) 1647–1654.
- [22] H.-P. Cong, S. Xin, S.-H. Yu, Flexible nitrogen-doped graphene/SnO₂ foams promise kinetically stable lithium storage, *Nano Energy* 13 (2015) 482–490.
- [23] R. Wang, C. Xu, J. Sun, L. Gao, H. Yao, Solvothermal-induced 3D macroscopic SnO₂/nitrogen-doped graphene aerogels for high capacity and long-life lithium storage, *ACS Appl. Mater. Interfaces* 6 (5) (2014) 3427–3436.
- [24] X. Zhou, L.J. Wan, Y.G. Guo, Binding SnO₂ nanocrystals in nitrogen-doped graphene sheets as anode materials for lithium-ion batteries, *Adv. Mater.* 25 (15) (2013) 2152–2157.
- [25] J. Sun, L. Xiao, S. Jiang, G. Li, Y. Huang, J. Geng, Fluorine-doped SnO₂@graphene porous composite for high capacity lithium-ion batteries, *Chem. Mater.* 27 (13) (2015) 4594–4603.
- [26] C. Zhang, X. Peng, Z. Guo, C. Cai, Z. Chen, D. Wexler, et al., Carbon-coated SnO₂/graphene nanosheets as highly reversible anode materials for lithium ion batteries, *Carbon* 50 (5) (2012) 1897–1903.
- [27] Y. Dong, Z. Zhao, Z. Wang, Y. Liu, X. Wang, J. Qiu, Dually fixed SnO₂ nanoparticles on graphene nanosheets by polyaniline coating for superior lithium storage, *ACS Appl. Mater. Interfaces* 7 (4) (2015) 2444–2451.
- [28] H. Ding, H. Jiang, Z. Zhu, Y. Hu, F. Gu, C. Li, Ternary SnO₂@PANI/rGO nano-hybrids as excellent anode materials for lithium-ion batteries, *Electrochim Acta* 157 (2015) 205–210.
- [29] H.A. Becerril, J. Mao, Z. Liu, R.M. Stoltenberg, Z. Bao, Y. Chen, Evaluation of solution-processed reduced graphene oxide films as transparent conductors, *ACS Nano* 2 (3) (2008) 463–470.
- [30] S. Ding, D. Luan, F.Y. Boey, J.S. Chen, X.W. Lou, SnO₂ nanosheets grown on graphene sheets with enhanced lithium storage properties, *Chem. Commun.* 47 (25) (2011) 7155–7157.
- [31] T. Zhang, H. Chang, Y. Wu, P. Xiao, N. Yi, Y. Lu, et al., Macroscopic and direct light propulsion of bulk graphene material, *Nat. Phot.* 9 (7) (2015) 471–476.
- [32] Y. Huang, D. Wu, S. Han, S. Li, L. Xiao, F. Zhang, et al., Assembly of tin oxide/graphene nanosheets into 3D hierarchical frameworks for high-performance lithium storage, *ChemSusChem* 6 (8) (2013) 1510–1515.
- [33] Y. Wu, N. Yi, L. Huang, T. Zhang, S. Fang, H. Chang, et al., Three-dimensionally bonded spongy graphene material with super compressive elasticity and near-zero Poisson's ratio, *Nat. Commun.* 6 (2015) 6141.
- [34] F. Zhang, X. Yang, Y. Xie, N. Yi, Y. Huang, Y. Chen, Pyrolytic carbon-coated Si nanoparticles on elastic graphene framework as anode materials for high-performance lithium-ion batteries, *Carbon* 82 (0) (2015) 161–167.
- [35] Y. Zhang, Y. Huang, T. Zhang, H. Chang, P. Xiao, H. Chen, et al., Broadband and tunable high-performance microwave absorption of an ultralight and highly compressible graphene foam, *Adv. Mater.* 27 (12) (2015) 2049–2053.
- [36] X. Wang, X. Zhou, K. Yao, J. Zhang, Z. Liu, A SnO₂/graphene composite as a high stability electrode for lithium ion batteries, *Carbon* 49 (1) (2011) 133–139.
- [37] S.J. Prabar, Y.H. Hwang, E.G. Bae, S. Shim, D. Kim, M.S. Lah, et al., SnO₂(/graphene composites with self-assembled alternating oxide and amine layers for high Li-storage and excellent stability, *Adv. Mater.* 25 (24) (2013) 3307–3312.
- [38] D.O. Shin, H. Park, Y.-G. Lee, K.M. Kim, T.H. Han, Direct hybridization of tin oxide/graphene nanocomposites for highly efficient lithium-ion battery anodes, *J. Electroceram.* 33 (3–4) (2014) 195–201.
- [39] J. Zhang, L. Chang, F. Wang, D. Xie, Q. Su, G. Du, Ultrafine SnO₂ nanocrystals anchored graphene composites as anode material for lithium-ion batteries, *Mater. Res. Bull.* 68 (2015) 120–125.
- [40] Z. Chen, M. Zhou, Y. Cao, X. Ai, H. Yang, J. Liu, In situ generation of few-layer graphene coatings on SnO₂-SiC core-shell nanoparticles for high-performance lithium-ion storage, *Adv. Energy Mater.* 2 (1) (2012) 95–102.
- [41] D. Wang, J. Yang, X. Li, D. Geng, R. Li, M. Cai, et al., Layer by layer assembly of sandwiched graphene/SnO₂ nanorod/carbon nanostructures with ultrahigh lithium ion storage properties, *Energy Environ. Sci.* 6 (10) (2013) 2900.
- [42] Z. Wang, D. Luan, S. Madhavi, Y. Hu, X.W. Lou, Assembling carbon-coated [small alpha]-Fe₂O₃ hollow nanohorns on the CNT backbone for superior lithium storage capability, *Energy Environ. Sci.* 5 (1) (2012) 5252–5256.
- [43] X. Zhou, Z. Dai, S. Liu, J. Bao, Y.G. Guo, Ultra-uniform SnO_x/carbon nanohybrids toward advanced lithium-ion battery anodes, *Adv. Mater.* 26 (23) (2014) 3943–3949.